A Markov Chain Random Asymmetrical SVPWM Method to Suppress High-Frequency Harmonics of Output Current in an IMC-PMSM System

Yang Yang, Weizhang Song, Yang Ge, and Patrick Wheeler, *Fellow, IEEE*

***Abstract*—In the system of permanent magnet synchronous motor (PMSM) driven by indirect matrix converter (IMC), space vector pulsewidth modulation (SVPWM) technology is used in the inverter stage, which causes that the output current generates high-frequency harmonics around the integral multiples carrier frequency, thus generating high-frequency noise and electromagnetic interference. In order to suppress the high-frequency harmonics of output current in IMC-PMSM, a Markov chain random asymmetrical SVPWM (MRA-SVPWM) method is proposed in this article. Although random PWM (RPWM) technology have some effect to reduce the harmonic amplitude. There are still some inherent defects. Markov chain with nonaftereffect is applied to random switching frequency PWM in order to improve the performance of RPWM. Meanwhile, MRA-SVPWM changes the switching state by adjusting the vectors order and, thus, changes the coefficient of the harmonic. A better suppression performance around the integer multiples carrier frequency is achieved. Meanwhile, the principle of harmonic suppression is analyzed by using three-dimensional Fourier. Finally, the effectiveness of the proposed algorithm is verified by experiments.**

***Index Terms*—Harmonics suppression, indirect matrix converter (IMC), permanent magnet synchronous motor (PMSM), random PWM (RPWM).**

I. Introduction

RECENTLY, the indirect matrix converter (IMC) has attracted widely attention due to the superior input and output performance, bidirectional energy flow, and nonlarge-capacitors in the dc-side [1]. And IMC is widely used in various industry applications, especially three-phase ac driven system [2], [3]. On the other hand, permanent magnet synchronous motor (PMSM) is widely used as the driven motor in ac drive system due to the advantages of high power density, high efficiency, small size, and wide speed range. It is now widely used in various industries such as rail transportation and machinery manufacturing [4], [5], [6].

At present, in the IMC-PMSM system, the space vector pulsewidth modulation (SVPWM) technology is commonly used, which has achieved good results. However, there are still some unresolved problems. It prone to lead the large harmonic amplitude around the integer multiples carrier frequency in the stator current [7]. Then resulting in high-frequency noise and electromagnetic interference [8]. In many special industrial applications, the requirement for motor noise, which caused by high-frequency harmonics is very strict. Therefore, it is necessary to reduce the adverse impact of high-frequency harmonics to the system.

Some new modulation technologies to suppress the harmonics have been proposed. The interleaved parallel inverter structure has a good effect on harmonics suppression [9], [10]. Although this is available in parallel in IMC, it increases the number of inverters and cost.

Random PWM (RPWM), which includes random pulse position random center distribution (RCD) [11], random zero voltage vector distribution (RZD), and random switching frequency (RSF) PWM [12] can disperse the superimposed harmonics throughout the spectrum through random processing of the switching position and the switching frequency, so as to suppress the higher harmonics to reduce the motor noise [13]. Zhang et al. [14] proposed RCDPWM with equal probability of randomly selecting N carrier modes in each carrier cycle to obtain different pulse position state. However, the implementation of RCDPWM is more complicated. Peyghambari et al. [15] proposed a new RPWM based on the relation between the reference rotary vector and switching periods in order to create a gap in the line voltage power spectrum density of three-phase inverter to reduce the acoustic noise and vibration. In [16], a hybrid PWM strategy of RSF and RCD was proposed to be applied to a five-phase inverter to suppress high-frequency harmonics. Although RFSPWM is effective in harmonic suppression, it is extremely dependent on the distribution effect of the random number. If the range of random number is too small, the motor efficiency and the effect of harmonic suppression will be reduced, conversely, the switching loss will be increased.

Besides the interleaved parallel inverter structure and RPWM, the modified SVPWM provides another way to reduce the

Manuscript received 4 March 2023; revised 8 June 2023 and 8 August 2023; accepted 2 September 2023. Date of publication 8 September 2023; date of current version 6 December 2023. This work was supported in part by the National Natural Science Foundation of China under Grant 51877176, in part by the Key Research and Development Program of Shaanxi Province under Grant 2021GY-293, and in part by Science and Technology Planning Project of Xi'an under Grant 22GXFW0085. Recommended for publication by Associate Editor A. Trzynadlowski. *(Corresponding author: Weizhang Song.)*

Yang Yang, Weizhang Song, and Yang Ge are with the Department of Power Electronics and Motor, Xi'an University of Technology, Xi'an 710054, China (e-mail: 18092064658@163.com; swz@xaut.edu.cn; gy@xaut.edu.cn).

Patrick Wheeler is with the Department of Electrical and Electronic Engineering, University of Nottingham, NG7 2RD Nottingham, U.K. (e-mail: pat.wheeler@nottingham.ac.uk).

Color versions of one or more figures in this article are available at https://doi.org/10.1109/TPEL.2023.3313107.

Digital Object Identifier 10.1109/TPEL.2023.3313107

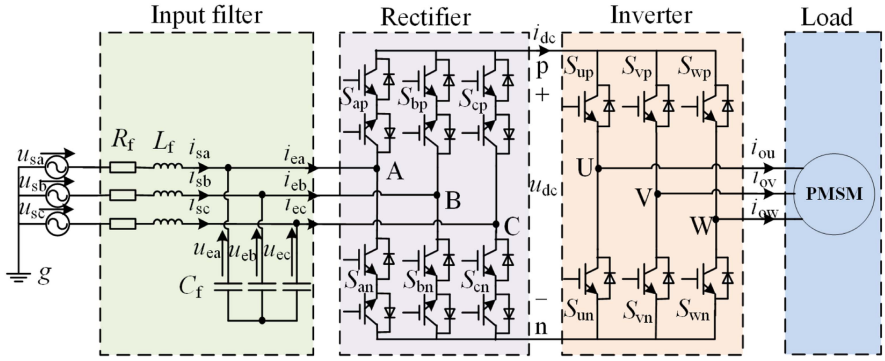

Fig. 1. IMC-PMSM topology.

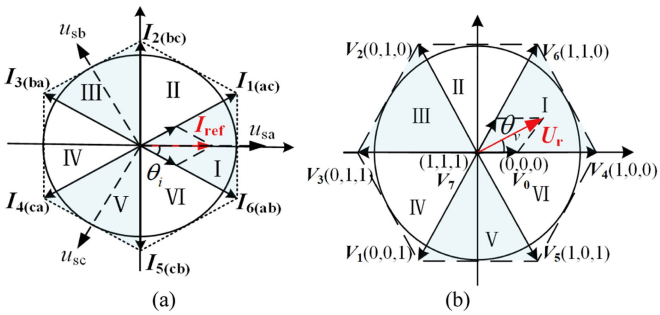

Fig. 2. Space vector diagrams for SVPWM. (a) Rectifier stage. (b) Inverter stage.

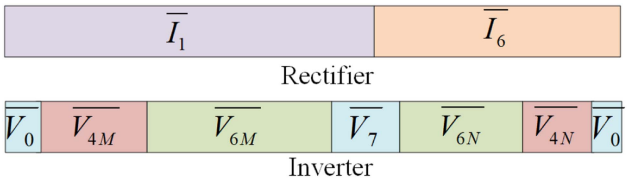

Fig. 3. Vector distribution of IMC rectifier-inverter coordinated commutation strategy.

TABLE I
RELATIONSHIP BETWEEN SECTOR AND DC VOLTAGE

Sector	Angle	Open switch	Modulation switch	Dc voltage
1	-π/6~π/6	S_{ap}	S_{bn}, S_{cn}	u_{ab}, u_{ac}
2	π/6~π/2	S_{cn}	S_{ap}, S_{bp}	u_{ac}, u_{bc}
3	π/2~5π/6	S_{bp}	S_{an}, S_{cn}	u_{ba}, u_{bc}
4	5π/6~7π/6	S_{an}	S_{bp}, S_{cp}	u_{ba}, u_{ca}
5	7π/6~9π/6	S_{cp}	S_{bn}, S_{an}	u_{cb}, u_{ca}
6	9π/6~11π/6	S_{bn}	S_{ap}, S_{cp}	u_{ab}, u_{cb}

harmonics by changing the pulse wave rules [17], [18]. Huang et al. [19], [20], and Han et al. [21] proposed the modified single-edge and double-edge regular sampling SVPWM technology, respectively. It modified switching state functions based on SVPWM, and combined with RSFPWM into a hybrid PWM technology. This method can change the harmonics coefficient. It is effective to reduce the harmonics at odd multiples of the carrier frequency, but increase that at even multiples.

This article proposes a better solution using Markov chain random asymmetrical SVPWM (MRA-SVPWM) method for high-frequency harmonics suppression of output current in an IMC-PMSM system. The goal of this method is to give the best performance in terms of the even distribution of harmonics on the frequency spectrum. By changing the random carrier frequency distribution and increasing the equivalent switching frequency, the harmonic amplitude around integer multiples carrier frequency are significantly reduced and it is beneficial to reduce the high-frequency noise of the motor. Meanwhile, the principle of harmonic suppression is analyzed by using three-dimensional (3-D) Fourier. The correctness and effectiveness of the proposed method are verified by experimental results.

II. MODULATION STRATEGY AND HARMONIC ANALYSIS OF IMC-PMSM SYSTEM

A. Modulation Strategy

IMC is a kind of ac–dc–ac converter, whose structure is shown in Fig. 1. IMC consists of three parts: *LC* filter, rectifier stage and inverter stage. Generally, both rectifier and inverter adopt conventional SVPWM.

Conventional SVPWM divides sectors and decomposes reference vector into active vectors, which is shown in Fig. 2. By calculating and distributing the duty ratio of the active vectors, the switching states and driving pulses are obtained. The rectifier stage modulation strategy does not contain zero vector, while the inverter stage contains two zero vectors, whose duty ratios are shown as follows [22], shown at the bottom of next page.

$$\begin{cases} d_{i1} = m_i \sin(\frac{\pi}{3} - \theta_i) \\ d_{i2} = m_i \sin(\theta_i) \end{cases} \tag{1}$$

$$\begin{cases} d_{v1} = m_v \sin(\frac{\pi}{3} - \theta_v) \\ d_{v2} = m_v \sin(\theta_v) \\ d_0 = d_7 = \frac{1}{2}(1 - d_{v1} - d_{v2}) \end{cases} \tag{2}$$

where d_{i1}, d_{i2} and d_{v1}, d_{v2} are duty ratio of active vectors in the rectifier and inverter stage, d_0 and d_7 are the duty ratio of zero current vectors. m_i and m_v are the modulation index of the rectifier and inverter stage. θ_i and θ_v are the angle between

the reference vector and the active vectors in the rectifier and inverter stage.

In order to realize the zero current commutation of the rectifier stage, the vector distribution of the inverter stage needs to be reprogrammed to form a set of complete modulation strategy for the whole topology, which is shown in Fig. 3. The active current vectors of the rectifier stage are $\boldsymbol{I}_1$ and $\boldsymbol{I}_2$, and the corresponding duty ratio are d_{i1} and d_{i2}. The active voltage vectors of the inverter stage are $\boldsymbol{V}_1$ and $\boldsymbol{V}_2$, and the corresponding duty ratio are d_{v1} and d_{v2}. While the duty ratio of the zero vector $\boldsymbol{V}_0$ and $\boldsymbol{V}_7$ are d_0 and d_7. When zero vector appears in the inverter stage, the output side of which is connected to the P or N of the dc-side, and there is no current loop in the dc-side. At this time, the current vector of rectifier stage is switched, and there is no current flows through the switching tube. Therefore, the coordinated commutation of IMC can be achieved by changing the switching states of the rectifier stage within the zero vector action interval of the inverter stage, and the switching voltage peak of the rectifier stage can be effectively reduced.

B. Theoretical Analysis of High-frequency Harmonic of SVPWM

The high-frequency harmonics are mainly caused by the high-frequency inverter switches. In this section, its characteristic is analyzed briefly as follows.

The PWM time-varying function of harmonics components can be expressed, as shown in (3) at the bottom of this page [23], [24].

where $x = \omega_d + \theta_d, y = \omega_c + \theta_c$ and $z = \omega_0 + \theta_0$. $\omega_d\ \omega_c\ \omega_0$ are the angular frequency of the grid, carrier wave, and fundamental wave. $\theta_d\ \theta_c\ \theta_0$ are the initial angle of the grid, carrier wave, and fundamental wave. $k\ m\ n$ are the grid, carrier and baseband index variable. A_{kmn}, B_{kmn} are the coefficients of equation, which is shown in (4) at the bottom of this page.

In (3), harmonic components are divided into four parts: the first part on the right side of (3) represents the de component; the second represents the base band of harmonic component associated with the grid, carrier or the fundamental frequency; the third represents harmonic components between two frequencies; the fourth represents the harmonic components relevant to the grid, carrier or the fundamental frequency. The high-frequency harmonics concentrate at the frequency of $kf_d + mf_c \pm nf_0$. For example, $m = 1$ and $n = 2$ define the second sideband harmonic in the group of harmonics that are located around the first carrier harmonic. In industrial applications, it is necessary to pay attention to the harmonic components near the first and second order carrier frequency, i.e., $m = 1$ and $m = 2$. By 3-D Fourier integral, the harmonics amplitude within a fundamental frequency waveform period can be expressed as follows:

$$U_u = 2j(A_{kmn} + jB_{kmn}). \tag{5}$$

Since the inverter stage uses the SVPWM. The modulated wave of SVPWM can be defined as [25]

$$z(t) = a\left(\frac{2}{\sqrt{3}}\cos\omega t_0 + \sum_{k=0}^{\infty}\frac{6\times(-1)^{k+1}}{\pi(1-n^2)}\cos 3\omega t_0\right) \tag{6}$$

where $n = 6k + 3$, $k = 0, 1, 2,\ldots$ when $k \geq 1$, the harmonic coefficients are all very small compared with the fundamental one. Therefore, only the fundamental and third harmonics are considered in the study. The function z(t) can be approximated as

$$z(t) = M\cos\omega t_0 + M_3\cos 3\omega t_0 \tag{7}$$

where $M = \frac{2a}{\sqrt{3}}$,$M_3 = \frac{3\sqrt{3}}{8\pi}M$.

During a period of maximum dc side voltage. Using the double-edge symmetrical regular sampling technology. The expression of U_u can be redefined, as shown in (8) at the bottom of this page, where U_{im} is the max voltage in grid side. However, the integration limits are related to the sector number of reference

$$f(x,y,z) = \frac{A_{000}}{2} + \begin{bmatrix} \sum_{k=1}^{\infty}(A_{k00}\cos kx + B_{k00}\sin kx) \\ + \sum_{m=1}^{\infty}(A_{0m0}\cos my + B_{0m0}\sin my) \\ + \sum_{n=1}^{\infty}(A_{00n}\cos nz) + B_{0n}\sin nz) \end{bmatrix} + \begin{bmatrix} \sum_{k=1}^{\infty}\sum_{m=1}^{\infty}[A_{km0}\cos(kx+my) + B_{km0}\sin(kx+my)] + \\ \sum_{k=1}^{\infty}\sum_{\substack{n=-\infty \\ (n\neq 0)}}^{\infty}[A_{k0n}\cos(kx+nz) + B_{k0n}\sin(kx+nz)] + \\ \sum_{m=1}^{\infty}\sum_{\substack{n=-\infty \\ (n\neq 0)}}^{\infty}[A_{0mn}\cos(my+nz) + B_{0mn}\sin(my+nz)] \end{bmatrix}$$
$$+ \sum_{k=1}^{\infty}\sum_{m=1}^{\infty}\sum_{\substack{n=-\infty \\ (n\neq 0)}}^{\infty}[A_{kmn}\cos(kx+my+nz) + B_{0mn}\sin(kx+my+nz)] \tag{3}$$

$$A_{kmn} + jB_{kmn} = \frac{1}{4\pi^3}\int_0^{2\pi}\int_0^{2\pi}\int_0^{2\pi} f(x,y,z)e^{j(kx+my+nz)}\mathrm{d}x\mathrm{d}y\mathrm{d}z \tag{4}$$

$$A_{kmn} + jB_{kmn} = \frac{3}{8\pi^3}\int_{-\frac{\pi}{6}}^{\frac{\pi}{6}}\int_{-\pi}^{\pi}\int_{-\frac{\pi}{2}(M\cos z + M_3\gamma\cos 3z + 1)}^{\frac{\pi}{2}(M\cos z + M_3\gamma\cos 3z + 1)} U_{im}e^{j(kx+my+nz)}\mathrm{d}x\mathrm{d}y\mathrm{d}z \tag{8}$$

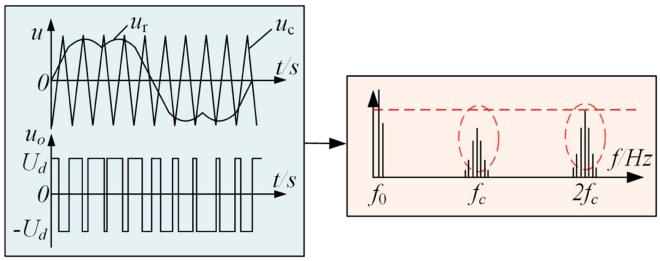

Fig. 4. Diagram of the effect of conventional SVPWM and frequency spectrum.

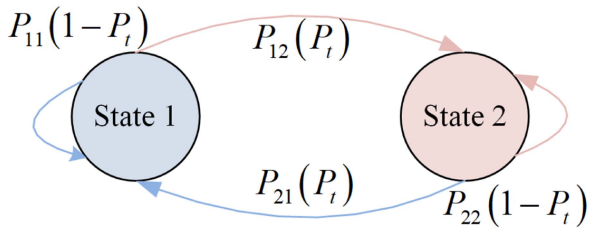

Fig. 5. Diagram of state transition.

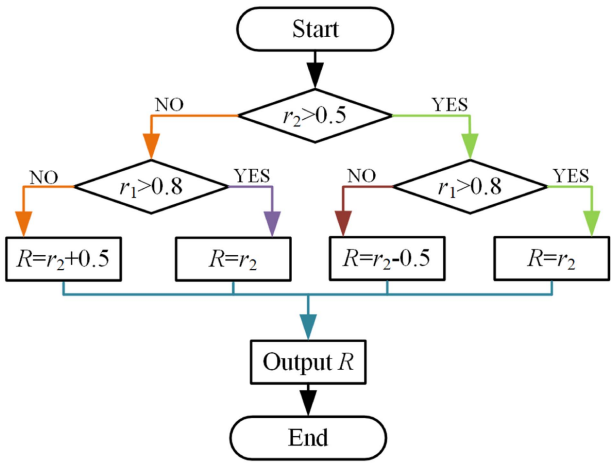

Fig. 6. Random number generation flowchart of two-state Markov chain.

TABLE II
RANDOM NUMBER EVALUATION STANDARD PARAMETERS

	Conventional random numbers	Markov chain random numbers
Total sample size	100	100
Actual mathematical expectation in (13)	0.526164	0.506985
Deviation degree D' in (14)	0.215036	0.262285
Asymptotic Significance of normal distribution	0.169	0.011
Asymptotic Significance of uniform distribution	0.37	0.698
Asymptotic Significance of Poisson distribution	0.00	0.00

input current vector. In order to obtain the maximum dc side voltage, it is necessary to divide the sectors of input voltage at the grid side. In each sector, to ensure that the switch tube with one phase bridge arm is always on, the voltage amplitude of this phase must be the maximum; while the other two-phase switch tube is modulated, and its voltage polarity is opposite to the former and there are intersection points. The relationship between sector and dc voltage is shown is Table I, shown at the bottom of next page.

To sum up, he main harmonic components are distributed around the integer multiples carrier frequency harmonics and its sideband harmonics under conventional SVPWM, which is shown in Fig. 4. Only a small amount of the integer multiple harmonics of the fundamental frequency are contained, which is the low frequency harmonics.

It is known above that the harmonics contents are mainly determined by coefficients A_{mn}, B_{mn}, carrier frequency ω_c and fundamental frequency ω_0. Therefore, the harmonics can be suppressed by changing the carrier frequency, reducing the coefficient, and changing the control strategy.

III. MRA-SVPWM

As described previously, the output load of IMC generates high-frequency harmonics due to the effect of the inverter switches under SVPWM. In this section, a Markov chain random asymmetrical SVPWM (MRA-SVPWM) technology is proposed to suppress high-frequency harmonics at the first and second order carrier frequency.

A. Markov Chain RPWM

The random algorithm is applied to the variable frequency speed control system. The random frequency can be obtained by [16]

$$f_s = f_0 \pm \Delta f \cdot R \tag{9}$$

where f_s is the random switching frequency, f_0 is the fixed switching frequency, Δf is the random gain, and R is the random number, which is generated by the linear congruence method

$$R_{n+1} = \mathrm{mod}2^{Ns}(R_n \times P_1 + P_2) \tag{10}$$

where R_n and R_{n+1} represent random numbers generated at the nth and $(n+1)$th times, respectively. N_S represents random number digits, and P_1 and P_2 are two prime numbers.

In general, in order to show better performance of random numbers, the number of random numbers would be increased, which requires longer recursive formulas and periods, so 0, 1, …, $2N_s$-1 These numbers will appear in the full period. Random number $R_{(0)}$ can take any integer value from 0 to $2N_s$-1, and the sufficient and necessary conditions for the full period are that the first initial value P_1 is in the form of $4K+1$ (K is a non-negative integer number), and the second initial value P_2 is a mutual prime with 2^{Ns}. Therefore, $P_1 = 29$ and $P_2 = 37$ are selected to be implemented in the 16-bit microprocessor. In order to facilitate application in RPWM strategy and performance evaluation, random number unit within the range of 0∼1. Here,

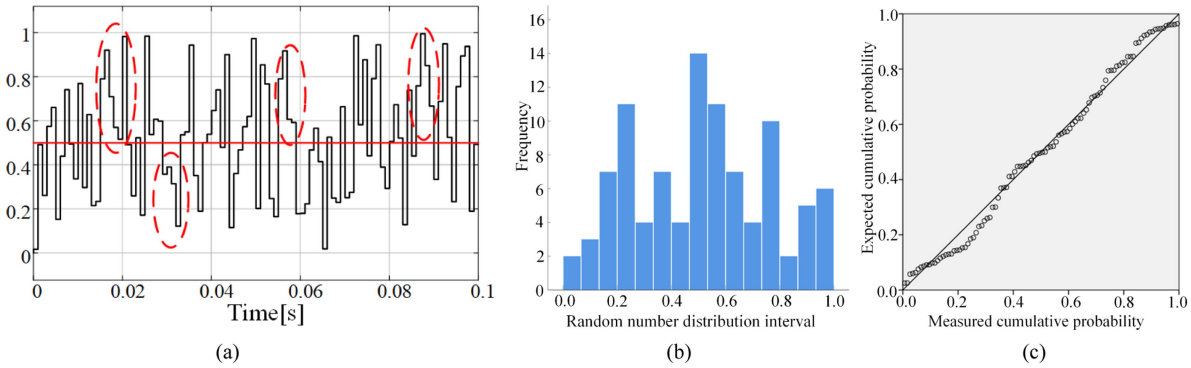

Fig. 7. Distribution diagram, histogram and P-P plot of conventional random number. (a) Distribution diagram. (b) Histogram. (c) P-P plot.

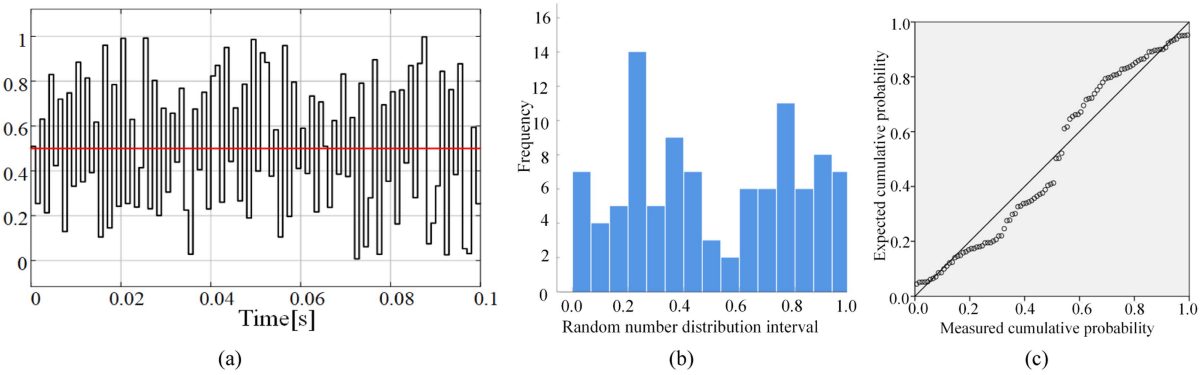

Fig. 8. Distribution diagram, histogram, and P-P plot of Markov chain random numbers. (a) Distribution diagram. (b) Histogram. (c) P-P plot.

$P_1 = 29$, $P_2 = 37$ and $N_s = 16$ are chosen for random number generation. The random number generation equation is shown as follows:

$$R_{n+1} = [\mathrm{mod}2^{16}(R_n \times 29_1 + 37)]/65535. \quad (11)$$

The following paper shows the distribution of 100 random numbers generated by conventional linear congruence method, which is used for RSFPWM. There is a tendency for random numbers generated at successive times to be distributed on the same side of the mathematical expectation and worse distribution, which could make the harmonic distribution effect in the spectrum be poor. So, Markov chain is embedded into RSFPWM to obtain a better performance for distribution of random number.

Markov is a typical process with nonaftereffect, which can be understood as follows: The future state is only related to the present moment state instead of the past moment state. Define the transition probability matrix to describe the relationship between the present state and the next state [26]

$$P_{ij}(n-m) = P_{ij}(m,n) = P\{X_n = a_j \,|X_m = a_i\} = P\{X_n = j \,|X_m = i\} \quad i,j \in S \quad (12)$$

where P_{ij} (m, n) is the transfer probability that the state a_j at the n moment if the state a_i at the m moment.

Because of the Markov chain characteristic, the transfer probability is independent of the departure moment, and is only related to the states at the departure and arrival moments. When n-m = 1, $P_{ij}(1)$ is called to the one-step transfer probability, which is used in this article.

Considering the distribution of random switching frequency, two states are introduced here: 1) less than the expected switching frequency (state 1); 2) greater than the expected switching frequency (state 2). The two-state Markov chain is applied to RSFPWM, and its transfer process is shown in Fig. 5. P_1 = 29, P_2 = 37, and P_1 = 97, P_2 = 59 are prime numbers that generate two sets of random numbers r_1 and r_2. Defining the generated random number for the transition probability judgment is r_1. And the random number for random switching frequency is r_2. In order to select a more appropriate value of transfer probability, the performance of Markov chain random numbers under different P_t are evaluated. Finally, the transfer probability P_t = 0.8 is selected in this paper. The random number process generated by two-state Markov chain is shown in Fig. 6, which requires switching between two groups of random numbers.

The distribution diagrams and histograms of the 100 random numbers generated by conventional random numbers and the Markov chain random numbers are shown in Figs. 7(a) and (b) and 8(a) and (b). The distribution diagrams takes into account the influence of process and time on the distribution of random

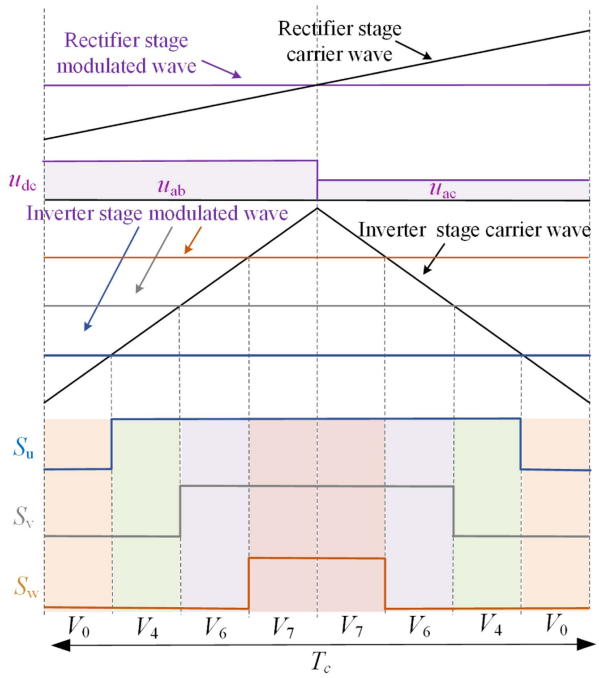

Fig. 9. Diagram of conventional SVPWM in sector 1.

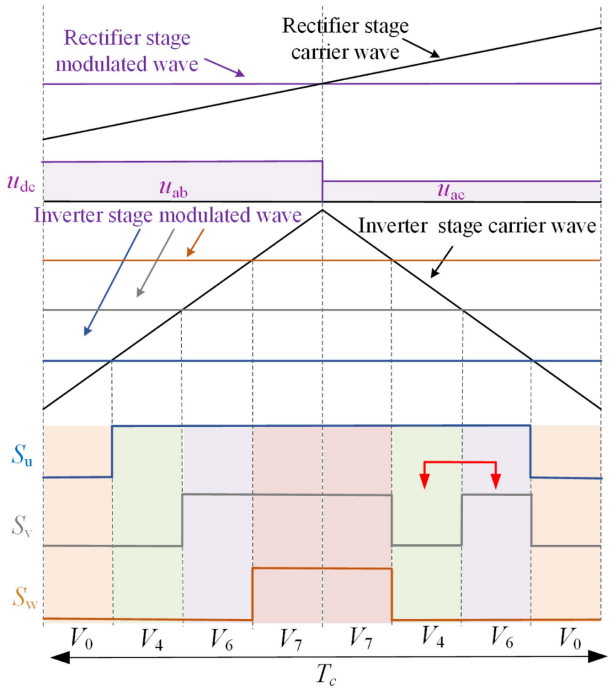

Fig. 10. Diagram of asymmetrical SVPWM in sector 1.

numbers, while the histograms do not take into account that and are intuitive expression of the distribution degree of statistics data. Therefore, it is necessary to consider the two factors of time dimension and numbers distribution degree to evaluate performance of random numbers. The theoretical random number range is 0.0∼1.0 and the theoretical mathematical expectation is 0.5. It can be seen from Figs. 7(a) and 8(a) that Markov

TABLE III
VECTORS ORDER OF ASYMMETRICAL SVPWM IN ALL SECTORS

Sector	Conventional SVPWM	Corresponding Bridge Arm	Asymmetrical SVPWM
I(0≤θ<60°)	0-4-6-7-7-6-4-0	S_v	0-4-6-7-7-4-6-0
II(60°≤θ<120°)	0-2-6-7-7-6-2-0	S_u	0-2-6-7-7-2-6-0
III(120°≤θ<180°)	0-2-3-7-7-3-2-0	S_w	0-2-3-7-7-2-3-0
IV(180°≤θ<240°)	0-1-3-7-7-3-1-0	S_v	0-1-3-7-7-1-3-0
V(240°≤θ<300°)	0-1-5-7-7-5-1-0	S_u	0-1-5-7-7-1-5-0
VI(300°≤θ<360°)	0-4-5-7-7-5-4-0	S_w	0-4-5-7-7-4-5-0

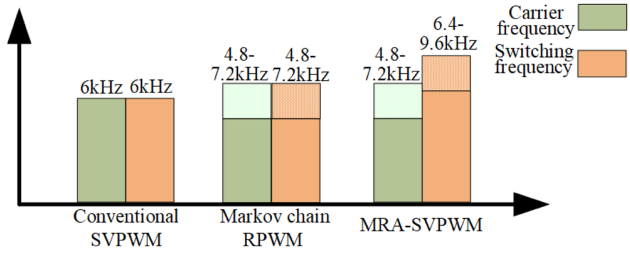

Fig. 11. Schematic diagram of carrier and switching frequency with conventional SVPWM, Markov chain RPWM, and MAR-SVPWM.

TABLE IV
PARAMETERS OF EXPERIMENT

Parameters	Values
Input voltage	100 V/50 Hz
Input filter	L_f=1.42 mH; C_f=30 μF
Rated power	3.7 kW
Pole pairs	4
Stator resistance	0.93 Ω
Stator inductance	9.1 mH
Rated speed	1000 r/min
Rotor inertia	0.01225 kg·m^2

TABLE V
COMPARISON OF HARMONICS AMPLITUDE WITH DIFFERENT ALGORITHMS

Algorithms	1 kHz		6 kHz	
	First order	Second order	First order	Second order
Conventional SVPWM	66 dB	73 dB	50 dB	56 dB
RCDPWM	57 dB	70 dB	45 dB	54 dB
RSFPWM	61 dB	66 dB	47 dB	49 dB
Hybrid PWM of RCD and RSF	58 dB	63 dB	45 dB	49 dB
Markov chain RPWM	57 dB	60 dB	42 dB	45 dB
MRA-SVPWM	53 dB	56 dB	39 dB	40 dB

chain random numbers avoid the tendency that random numbers generated at successive times to be distributed on the same side of the mathematical expectation. Meanwhile, it can be directly seen from the Figs. 7(b) and 8(b) that compared with conventional random, Markov chain random number avoids distribution near the theoretical mathematical expectation, which corresponds to the integer multiple switching frequency. It prefers to disperse harmonics throughout the spectrum, avoiding concentration near the integer multiple switching frequency

Meanwhile, in order to further verify the distribution and performance of random numbers. The mathematical expectation

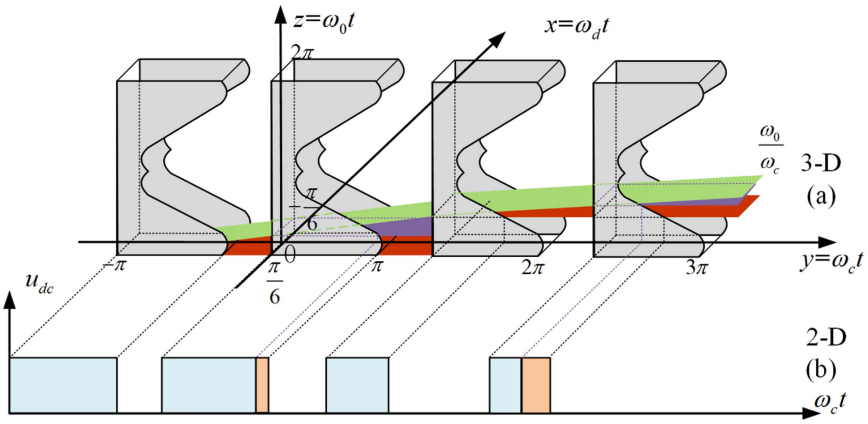

Fig. 12. Switching for the proposed MRA-SVPWM showing (a) staircase solution trajectory and (b) resultant switched PWM voltage.

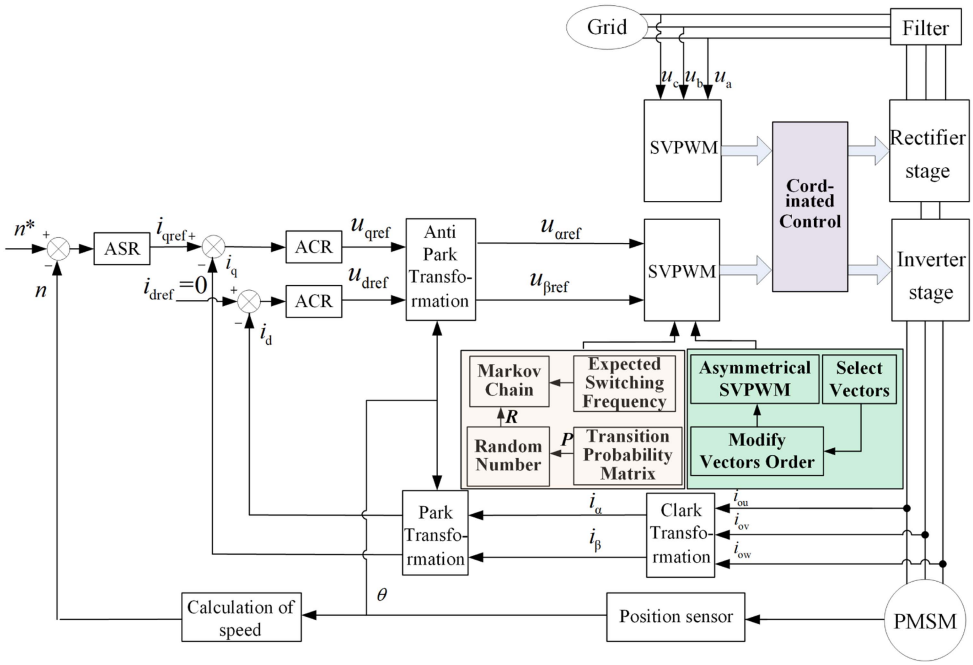

Fig. 13. Diagram of MRA-SVPWM in IMC-PMSM system.

and deviation degree are calculated through (13) and (14). Furthermore, we used statistical product and service solutions software to calculate probability statistics of random numbers. The inspection method used is One-Sample Kolmogorov–Smirnov Test. The mathematical expectation in (13), the deviation degree in through (14), asymptotic significance of normal, uniform, and Poisson distribution are tested and summarized in Table II

$$E[X] = \sum_i p_i x_i \tag{13}$$

where x_i is the value of random numbers and p_i is the probability corresponding to the random number

$$D'_n = \frac{1}{n} \sum_{i=1}^{\infty} |F_n(x_i) - F(x_i)| \tag{14}$$

where $F_n(x_i)$ is the distribution function to test sequence estimation and $F_n(x_i)$ is the theory of distribution function.

According to the results of test in Table II, the value of actual mathematical expectation is 0.526164 of conventional random numbers and 0.506985 of Markov chain random numbers. Compared with conventional random numbers, Markov chain random numbers are closer to theoretical mathematical expectations. It is benefit for random number performance. While ensuring the uniform distribution of switching frequency, it is closer to the desired frequency. The D' of conventional random numbers is 0.215036, and the D' of Markov chain random number is 0.262285. This verifies that the range of random number distribution based on Markov chain is more widely.

The values of asymptotic significance (Sig.) are 0.169 of conventional random numbers and 0.011 of Markov chain random

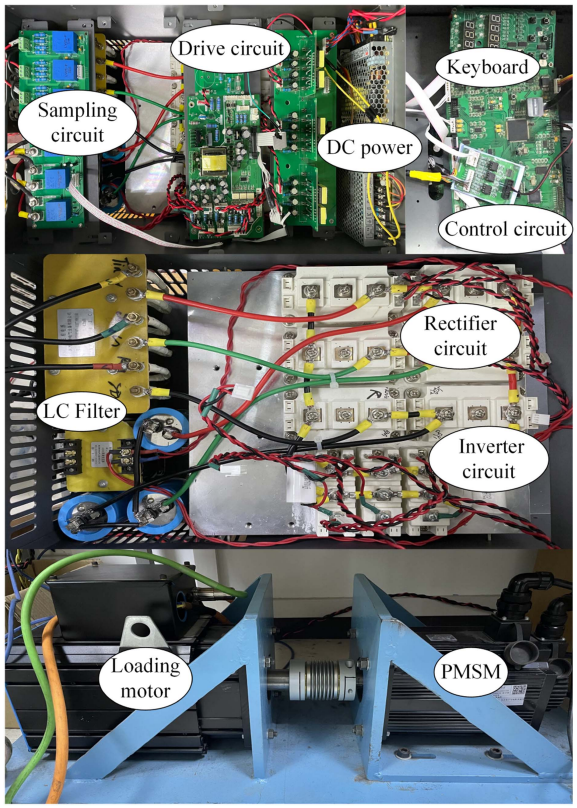

Fig. 14. Experimental prototype.

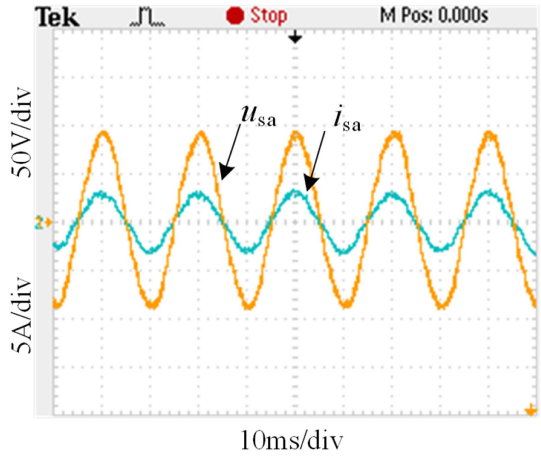

Fig. 15. Input phase voltage and current waveforms.

numbers. If the value of Sig. is greater than the significance level, which is generally default to 0.05, the null hypothesis is retained. The data can be considered subject to normal distribution. Otherwise, the null hypothesis is rejected and not subject to normal distribution. Hence, conventional random numbers are subject to normal distribution and Markov chain random numbers are not subject. Meanwhile, probability-probability plot (P-P plot) are drawn in Figs. 7(c) and 8(c), which is often used in probability and statistics discipline to evaluate whether a variable is subject to a normal distribution. P-P plot is a scatter plot drawn according to the cumulative probability of

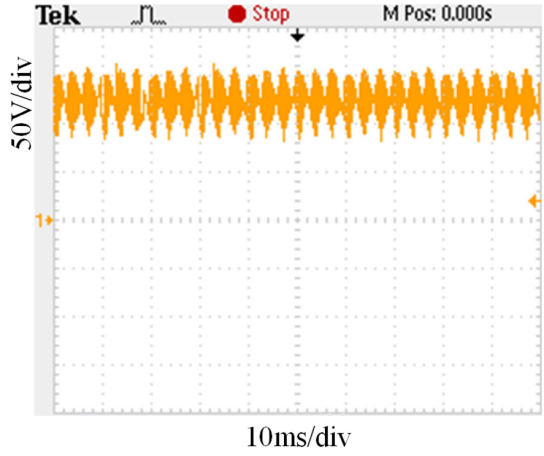

Fig. 16. DC-link voltage waveform.

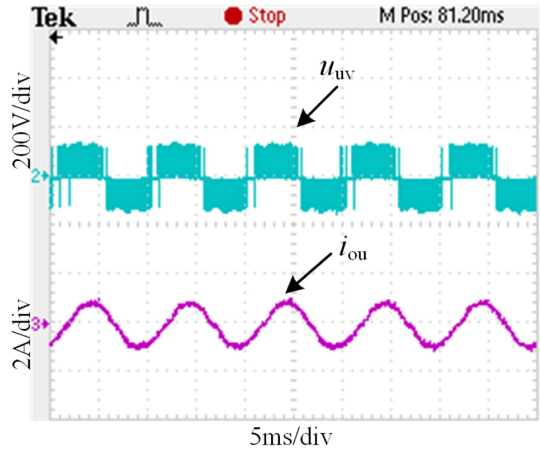

Fig. 17. Output line voltage and phase current waveforms.

variables corresponding to the specified theoretical distribution cumulative probability. The points representing the sample data should be roughly on the diagonal that represents the theoretical distribution. It can be seen from Fig. 7(c) that the distribution of conventional random numbers is distributed around the diagonal of the theoretical distribution. On the contrary, there are more Markov chain random numbers deviating from the diagonal in Fig. 8(c). Further illustrate that Markov chain random numbers have better distribution.

Similarly, the uniform and Poisson distribution are tested. The values of asymptotic significance (Sig.) are 0.37, 0.698 in uniform distribution and 0, 0 in Poisson distribution of random numbers based on conventional and Markov chain, respectively. The significance level is also default to 0.05. It can be concluded that both of them are subject to uniform distribution but not Poisson distribution.

In summary, only conventional random numbers are subject to normal distribution but the Markov chain random numbers are not. All random numbers are subject to uniform distribution but not Poisson distribution, and Markov chain random numbers have a wide distribution. Therefore, Markov chain random numbers have better performance in terms of randomness and distribution.

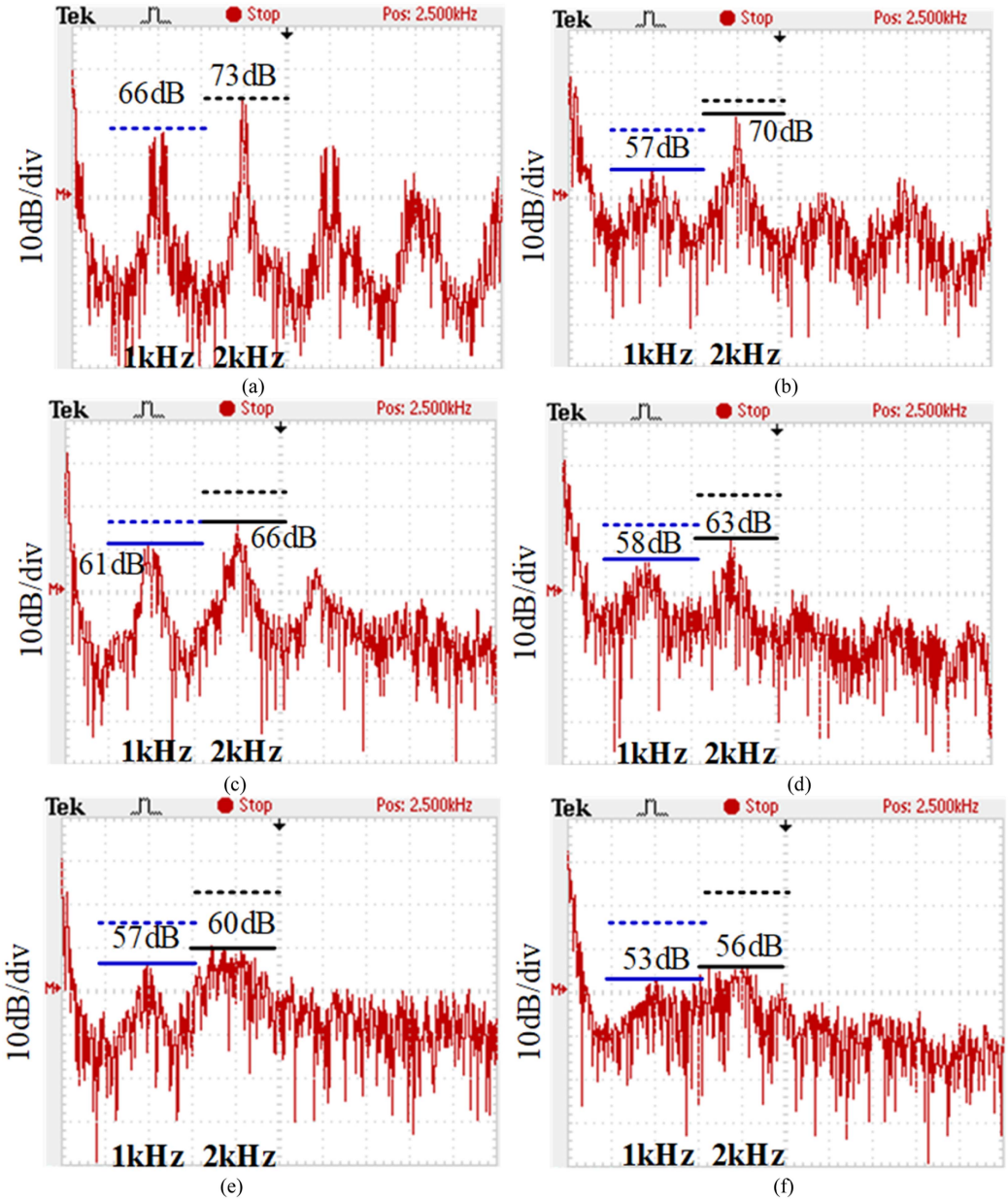

Fig. 18. Phase current FFT using different algorithms of 1 kHz carrier frequency. (a) Conventional SVPWM. (b) RCDPWM. (c) RSFPWM. (d) Hybrid PWM of RSF and RCD. (e) Markov chain RPWM. (f) MRA-SVPWM.

B. Asymmetrical SVPWM

Asymmetrical SVPWM can reduce the harmonic amplitude by increasing the equivalent switching frequency. Meanwhile, considering the switching state of the rectifier stage, this article considers the coordinated control of the front and rear stages. Asymmetrical SVPWM is realized by adjusting the active vectors order within half a cycle of the conventional SVPWM.

Taking the first sector as an example, the switching states and the vectors order of conventional SVPWM are shown in Fig. 9. In a carrier cycle, the active vectors order are symmetrical with respect to the intermediate vector$\boldsymbol{V_7}$ in the preceding and following half of a carrier cycle. The vectors order are $\boldsymbol{V_0}(000)\rightarrow\boldsymbol{V_4}(100)\rightarrow\boldsymbol{V_6}(110)\rightarrow\boldsymbol{V_7}(111)\rightarrow\boldsymbol{V_7}(111)\rightarrow\boldsymbol{V_6}(110)\rightarrow\boldsymbol{V_4}(100)\rightarrow\boldsymbol{V_0}(000)$. The three phase bridge arms of conventional SVPWM act for 2 times, so the total number of switching is 6.

The switching states of the asymmetrical SVPWM is shown in Fig. 10, and the vectors order are $\boldsymbol{V_0}(000)\rightarrow\boldsymbol{V_4}(100)\rightarrow\boldsymbol{V_6}(110)\rightarrow\boldsymbol{V_7}(111)\rightarrow\boldsymbol{V_7}(111)\rightarrow\boldsymbol{V_4}(100)\rightarrow\boldsymbol{V_6}(110)\rightarrow\boldsymbol{V_0}(000)$. Comparing the Figs. 9 and 10, it can be seen that in the preceding half of a carrier cycle, the switching order of conventional SVPWM and asymmetrical SVPWM is same exactly. But in the following half cycle, the vectors order of conventional SVPWM from $\boldsymbol{V_6}\rightarrow\boldsymbol{V_4}$ is changed to $\boldsymbol{V_4}\rightarrow\boldsymbol{V_6}$. The change in switching states is reflected in the driving pulse. The intermediate phase bridge arm acts for 4 times, and the other two phases bridge arms act for 2 times, so

the total number of switching within a cycle is 8. Compared with conventional SVPWM, the total switching frequency of asymmetrical SVPWM is increased by 33% with the same carrier frequency, and the switching sequences in other sectors is shown in Table III.

C. Markov Chain Random Asymmetrical SVPWM

Combining Markov chain RPWM and asymmetrical SVPWM into MRA-SVPWM technology, and applying it to the inverter modulation strategy. The proposed algorithm can suppress the harmonics and ensure the coordinated control of the rectifier and inverter stage. Markov chain RPWM is achieved by randomizing the carrier frequency, thus changing the distribution of harmonics on the spectrum determined by the carrier frequency. Markov chain random numbers have been introduced in Section III-A, and the carrier wave with variable frequency is generated by the random number generation method, thus, generates three phase PWM pulses. Asymmetrical SVPWM can be achieved by adjusting the vectors order in the second half-cycle. Markov chain processes the carrier wave, while asymmetrical SVPWM processes the signal wave, and the two algorithms are independent and uncoupled, shown at the bottom of this page.

In order to show the effect of different algorithms on switching frequency. Fig. 11 shows the carrier frequency and switching frequency using conventional SVPWM, Markov chain RPWM, and proposed MRA-SVPWM. When carrier frequency is 6 kHz, the switching frequency of conventional SVPWM is also 6 kHz. For Markov chain RPWM, random numbers were added, causing the carrier frequency to change. The switching frequency is consistent with the carrier frequency, they vary from 4.8 to 7.2 kHz. Due to increase the equivalent switching frequency by 33% and changing carrier frequency in MRA-SVPWM, comparing the carrier frequency of 4.8-7.2 kHz, the actual switching frequency varies from 6.4 to 9.6 kHz. Hence, the harmonics at integer multiple carrier frequency would be removed.

Due to changing the active vectors order, the harmonic component coefficients of asymmetrical SVPWM would be changed. The modulated wave and carrier of asymmetrical SVPWM are similar to the single edge regularly sampled SVPWM technology, which can be equivalent to the comparison of the periodic unit composed of the modulated wave on one side and the stepped step wave on the other side, as shown in Fig. 12. As time t unfolds, $z = \omega_0$ and $y = \omega_c$ define a straight plane in the y, z plane with slope $\omega_0/\omega_c = \gamma$ (which is the plane of purple color) carrier ratio (note that both the carrier and fundamental angles are assumed to be zero at time $t = 0$, or in other words both θ_0 and θ_c are zero for this discussion). Intersections of this plane with the boundary locus between the two switching voltage levels correspond to the actual switching instant for particular values of ω_0 and ω_c. The stepping period of the step wave is 2π, and the vertices of the step wave are all on the plane with slope $\omega_0/\omega_c = \gamma$ (which is the plane of purple color). The equation of the step wave is $z' = z + (\omega_0/\omega_c)y$, by replacing z with z', the regularly sampled is achieved.

Here, one cycle is an example. In a [-π, π] cycle, the preceding half of the cycle is single-edge regularly sampling (red plane). In the following half of the cycle, the switching function makes the sampling plane change. The sampling plane originally located in red becomes purple, and single edge regularly sampling is still used. Compared to before, the plane's position changes. The green plane is a plane with slope $\omega_0/\omega_c = \gamma$, the red plane vertex is at -π, and the purple plane is at 0. After sampling and projection to the $y0z$ plane, the orange color of the second part is eliminated. The PWM voltage contains two parts. Part 1 of bule is defined by (15) shown at the bottom of this page, part 2 of orange is defined by (16) shown at the bottom of this page.

In this article, the frequency control system of IMC-PMSM is mainly consisted of power grid, rectifier stage, inverter stage, and load PMSM. In rectifier stage, SVPWM is adopted to sample the input voltage and calculate the pulse signal to control the switching states of the rectifier stage, while the inverter stage adopts the SVPWM. Considering the output load is PMSM, the double closed-loop control strategy with $i_d = 0$ is used. Meanwhile, MRA-SVPWM is adopted and embedded into the IMC-PMSM system. Its control block diagram is shown in Fig. 13.

IV. Experiment Results

In order to verify the feasibility of the proposed algorithm on harmonic suppression. An IMC-PMSM system prototype platform for engineering applications was built, as shown in Fig. 14, and the experimental parameters are shown in Table IV.

A. System Experimental Results and Analysis

Fig. 15 shows the input phase voltage and phase current waveforms of the IMC-PMSM system. The sinusoidal degree of the input side waveform is good, verifying that the system has a good performance in terms of input power factor. Fig. 16 is the dc-link voltage waveform. There is no store

$$A_{kmn} + jB_{kmn} = \frac{3}{8\pi^3}\int_{-\frac{\pi}{6}}^{\frac{\pi}{6}}\int_{-\pi}^{\pi}\int_{-\pi}^{\frac{\pi}{2}(M\cos z' + M_3\cos 3z' - 1)} U_{im} e^{j(kx+my+(nz'+\frac{\omega_0}{\omega_c}y])}\mathrm{d}x\mathrm{d}y\mathrm{d}z' + \frac{3}{8\pi^3}\int_{-\frac{\pi}{6}}^{\frac{\pi}{6}}\int_{-\pi}^{\pi}\int_{0}^{\frac{\pi}{2}(M\cos z' + M_3\cos 3z' + 1)} U_{im} e^{j(kx+my+n[z'+\frac{\omega_0}{\omega_c}y])}\mathrm{d}x\mathrm{d}y\mathrm{d}z' \tag{15}$$

$$A_{kmn} + jB_{kmn} = \frac{3}{8\pi^3}\int_{-\frac{\pi}{6}}^{\frac{\pi}{6}}\int_{-\pi}^{\pi}\int_{\frac{\pi}{2}(M\cos(z'-\gamma\pi) + M_3\cos 3(z'-\gamma\pi) + 1)}^{\frac{\pi}{2}(M\cos z' + M_3\cos 3z' + 1)} U_{im} e^{j(kx+my+n[z'+\frac{\omega_0}{\omega_c}y])}\mathrm{d}x\mathrm{d}y\mathrm{d}z'. \tag{16}$$

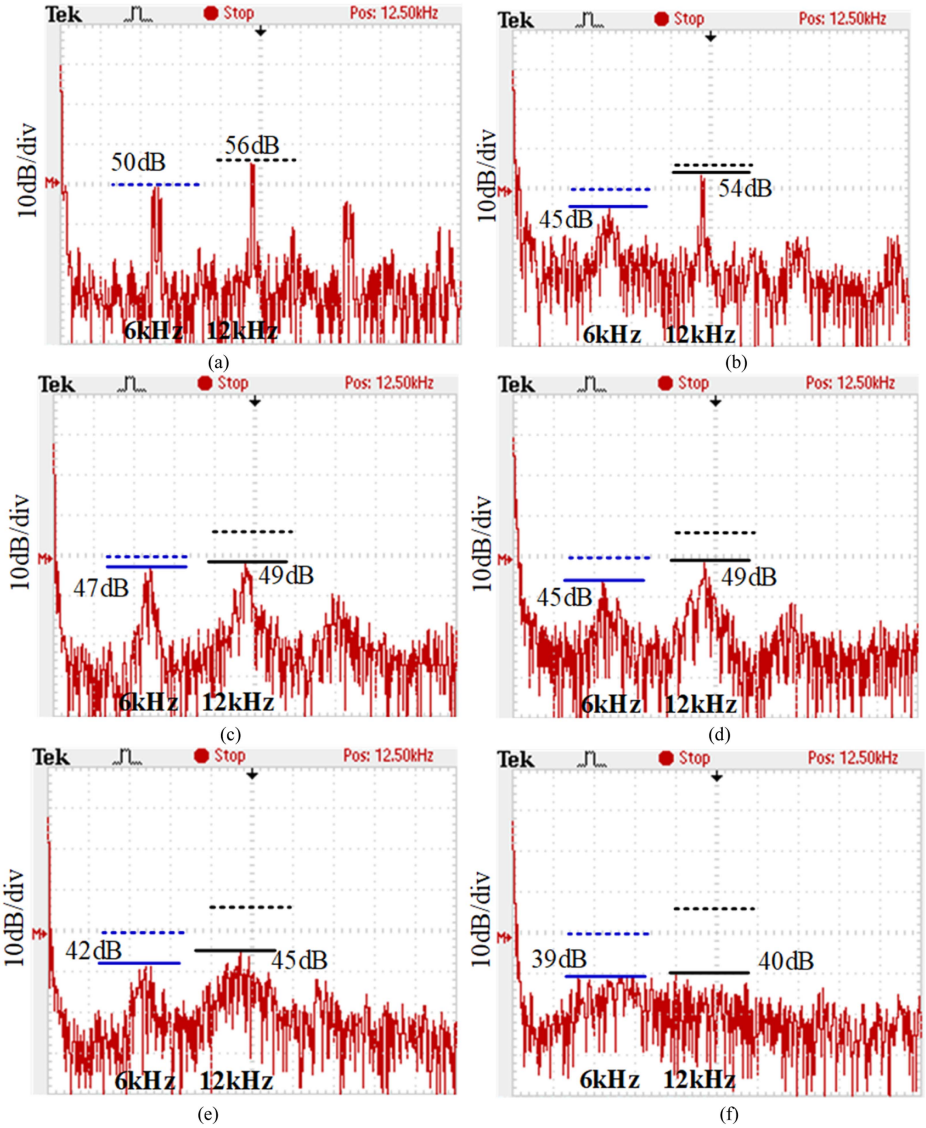

Fig. 19. Phase current FFT using different algorithms of 6 kHz carrier frequency. (a) Conventional SVPWM. (b) RCDPWM. (c) RSFPWM. (d) Hybrid PWM of RSF and RCD. (e) Markov chain RPWM. (f) MRA-SVPWM.

large capacitor in the dc side, so it is the positive pulsating voltage, which verifies the correctness of the modulation strategy in the rectifier stage. Fig. 17 shows the waveform of output line voltage and phase current. It can be seen that the system exhibits a good performance in terms of the transmission.

B. Harmonics Comparison of Different Algorithms

To verify the harmonics suppression effect, Figs. 18 and 19 show the phase current fast Fourier transform (FFT) using different algorithms at 1 kHz and 6 kHz carrier frequency, respectively. For special industrial applications, PMSM power usually reaches hundred and thousand kilowatts. In order to reduce switching losses, it is necessary to run at a low carrier frequency. Therefore, the lower (1 kHz) and higher (6 kHz) carrier frequency are chosen for experimental verification in this article. (a)–(e) are conventional SVPWM, RCDPWM, RSFPWM, hybrid PWM of RSF and RCD, Markov chain RPWM, and MRA-SVPWM proposed in the article, respectively. The dashed lines in the figures are the harmonics amplitude of conventional SVPWM, and the solid lines are the harmonics amplitude of different algorithms. The harmonics amplitudes of the first-order and second-order carrier frequencies are also summarized in Table V.

1) Conventional SVPWM: As shown in Figs. 18(a) and 19(a), there are the large harmonics amplitude at the integer multiple carrier frequency using conventional SVPWM. The lower the carrier frequency, the greater the harmonics amplitude. The level of the first-order and second-order carrier frequency harmonics are 66 dB, 73 dB and 50 dB, 56 dB at 1 kHz and 6 kHz carrier frequency.

2) RCDPWM: It can be seen from Figs. 18(b) and 19(b) that RCDPWM could reduce the harmonics amplitude by 9 dB, 3 dB and 5 dB, 2 dB at 1 kHz and 6 kHz carrier frequency.

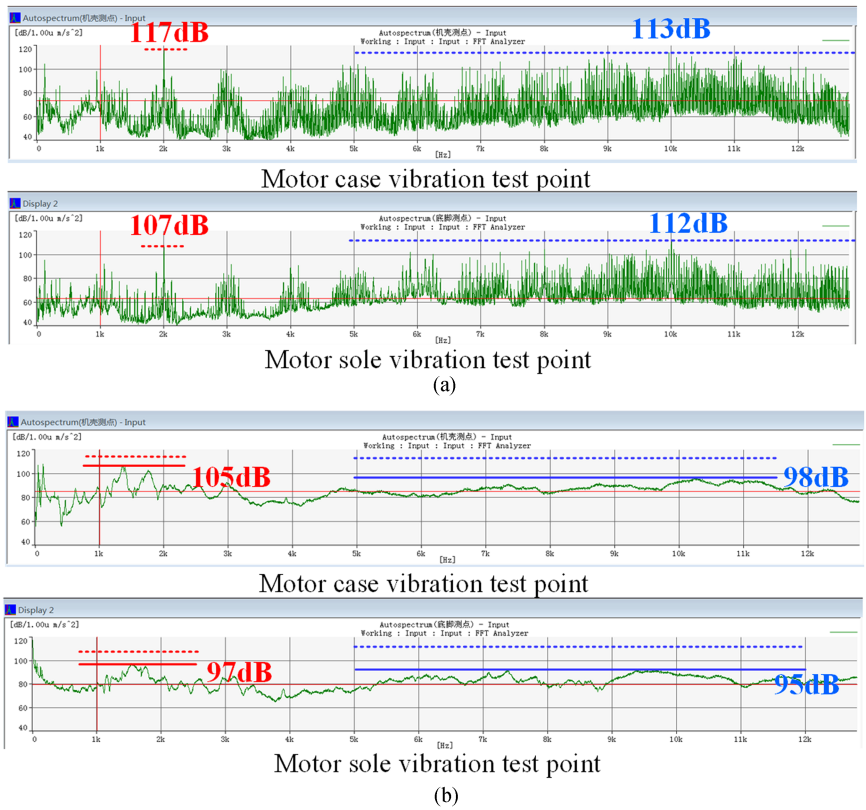

Fig. 20. Acoustic vibration waveform of 1 kHz carrier frequency. (a) Conventional SVPWM. (b) MRA-SVPWM.

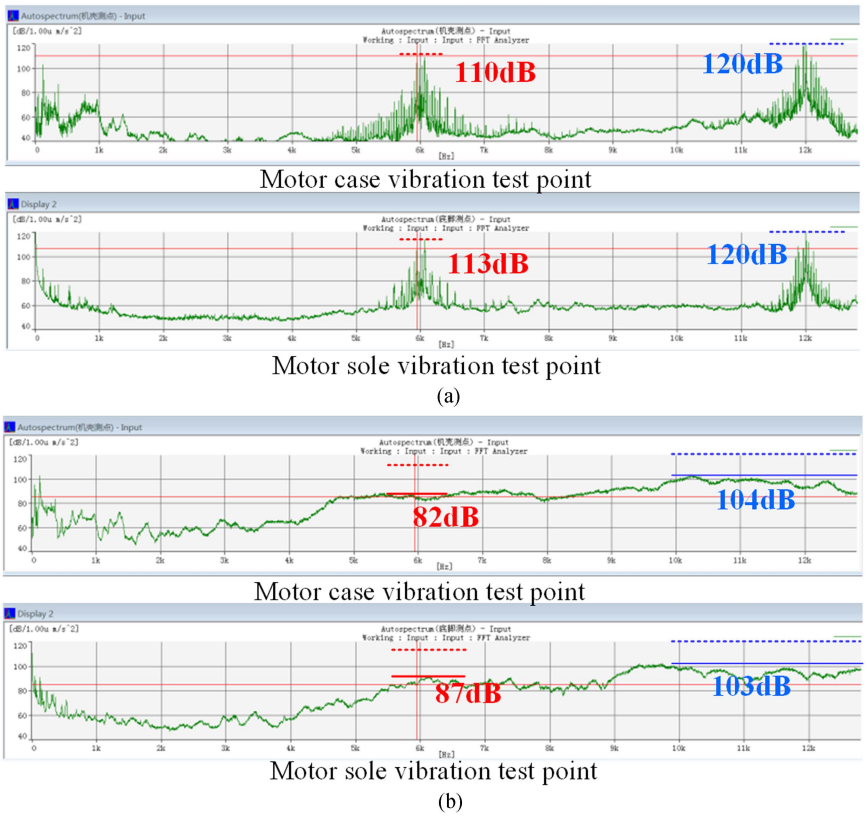

Fig. 21. Acoustic vibration waveform of 6 kHz carrier frequency. (a) Conventional SVPWM. (b) MRA-SVPWM.

It illustrates that RCDPWM could reduce the harmonics amplitude at first-order carrier frequency, while there is no significant suppression effect on second-order carrier frequency. Moreover, it has the tendency of harmonics moving to low frequency direction, which is detrimental to motor control performance.

3) RSFPWM: On the contrary, RSFPWM presents a better performance in terms of harmonics suppression at the second-order carrier frequency compared with first-order in Figs. 18(c) and 19(c). It reduces the harmonics amplitude by 5 dB, 7 dB and 3 dB, 7 dB at 1 kHz and 6 kHz carrier frequency. Whether RCDPWM or RSFPWM, the harmonic suppression effect at the integer multiple carrier frequency is limited.

4) Hybrid PWM of RCD and RSF: The hybrid PWM that combines the advantages of RCDPWM and RSFPWM is used shown in Figs. 18(d) and 19(d), which reduces the amplitude of harmonics by 8 dB, 10 dB and 5 dB, 7 dB at 1 kHz and 6 kHz carrier frequency. It can be seen that the hybrid algorithm has a better performance in terms of harmonic suppression comparing with the single algorithm. However, the suppression of harmonic amplitude is less than 10 dB. However, due to the addition of RCDPWM, the low frequency harmonics still increase.

5) Markov chain RPWM: In order to improve the randomness of random numbers, Markov chain is used for RSFPWM. The results of current FFT using Markov chain RPWM are shown in Figs. 18(e) and 19(e), which reduces the harmonics amplitude by 9 dB, 13 dB and 8 dB, 11 dB at 1 kHz and 6 kHz carrier frequency. It verifies that the Markov chain RPWM has a good effect on harmonic suppression. However, the reductions of harmonics amplitude at the integer multiple carrier frequency are also less than 10 dB.

6) MRA-SVPWM: The proposed MRA-SVPWM presents the best performance on harmonic suppression comparing five different RPWM algorithms. It can be seen proposed algorithm reduces the amplitude of harmonics by 13 dB, 16 dB and 11 dB, 16 dB at 1 kHz and 6 kHz carrier frequency from Figs. 18(f) and 19(f). It achieves the result of above 10 db suppression at all the integer multiple carrier frequency, which would be useful to reduce the motor noise. Moreover, it also avoids the increase of harmonic content at low frequencies like RCDPWM.

The acoustic vibration waveforms of motor case and sole test points at 1 kHz and 6 kHz carrier frequency were measured using conventional SVPWM and MRA-SVPWM by a high-precision vibration sensor shown in Figs. 20 and 21. The red line and numbers are amplitude of harmonics at the lower integer multiples carrier frequency. The blue line and numbers are amplitude and reduction of harmonics at frequency spectrum above 10 kHz. It can be seen from the results that proposed algorithm could reduce above 10 dB motor noise.

V. Conclusion

This article proposed a MRA-SVPWM method for high-frequency harmonics suppression in an IMC-PMSM system. In this method, Markov chain is embedded into RPWM by processing carrier wave to improve the random performance, thus, change the random carrier frequency distribution. Besides, the switching states are also adjusted by changing the vectors order to increase the equivalent switching frequency. The harmonics amplitude around integer multiples carrier frequency are reduced by proposed method. The experimental results show that the proposed method can suppress the high-frequency harmonic amplitude, so that the motor has a lower high-frequency noise. It can be widely used in industrial and transmission application where motor noise requirements are strict.

References

[1] J. W. Kolar, T. Friedli, J. Rodriguez, and P. W. Wheeler, "Review of three-phase PWM AC–AC converter topologies," *IEEE Trans. Ind. Electron.*, vol. 58, no. 11, pp. 4988–5006, Nov. 2011.

[2] M. Aguirre, S. Kouro, C. A. Rojas, and S. Vazquez, "Enhanced switching frequency control in FCS-MPC for power converters," *IEEE Trans. Ind. Electron.*, vol. 68, no. 3, pp. 2470–2479, Mar. 2021.

[3] W. Song, Y. Yang, W. Qin, and P. Wheeler, "Switching state selection for model predictive control based on genetic algorithm solution in an indirect matrix converter," *IEEE Trans. Transp. Electrific.*, vol. 8, no. 4, pp. 4496–4508, Dec. 2022.

[4] Y. Zhang, Z. Yin, X. Cao, Y. Zhang, and J. Liu, "A novel SPMSM sensorless drive using discrete-time synchronous-frequency adaptive observer under low frequency ratio," *IEEE Trans. Power Electron.*, vol. 37, no. 9, pp. 11045–11057, Sep. 2022.

[5] Y. Ge, L. Yang, and X. Ma, "A harmonic compensation method for SPMSM sensorless control based on the orthogonal master-slave adaptive notch filter," *IEEE Trans. Power Electron.*, vol. 36, no. 10, pp. 11701–11711, Oct. 2021.

[6] S. V. Nair, P. Harikrishnan, and K. Hatua, "Six-step operation of a symmetric dual three-phase PMSM with minimal circulating currents for extended speed range in electric vehicles," *IEEE Trans. Ind. Electron.*, vol. 69, no. 8, pp. 7651–7662, Aug. 2022.

[7] A. Ruiz-Gonzalez, F. Vargas-Merino, J. R. Heredia-Larrubia, M. J. Meco-Gutierrez, and F. Perez-Hidalgo, "Application of slope PWM strategies to reduce acoustic noiseradiated by inverter-fed induction motors," *IEEE Trans. Ind. Electron.*, vol. 60, no. 7, pp. 2555–2563, Jul. 2013.

[8] M. Farasat, A. Arabali, and A. M. Trzynadlowski, "Flexible-voltage DC-bus operation for reduction of switching losses in all-electric ship power systems," *IEEE Trans. Power Electron.*, vol. 29, no. 11, pp. 6151–6161, Nov. 2014.

[9] Y. Huang, Y. Xu, W. Zhang, and J. Zou, "Hybrid RPWM technique based on modified SVPWM to reduce the PWM acoustic noise," *IEEE Trans. Power Electron.*, vol. 34, no. 6, pp. 5667–5674, Jun. 2019.

[10] Y. Xu, W. Zhang, Y. Huang, and J. Zou, "Multisector three-phase PMSM drive system with low-frequency and high-frequency PWM noise," *IEEE J. Emerg. Sel. Topics Power Electron.*, vol. 10, no. 2, pp. 1639–1648, Apr. 2022.

[11] S.-Y. Oh, Y.-G. Jung, S.-H. Yang, and Y.-C. Lim, "Harmonic-spectrum spreading effects of two-phase random centered distribution PWM (DZRCD) scheme with dual zero vectors," *IEEE Trans. Ind. Electron.*, vol. 56, no. 8, pp. 3013–3020, Aug. 2009.

[12] K. Lee, G. Shen, W. Yao, and Z. Lu, "Performance characterization of random pulse width modulation algorithms in industrial and commercial adjustable-speed drives," *IEEE Trans. Ind. Appl.*, vol. 53, no. 2, pp. 1078–1087, Mar./Apr. 2017.

[13] P. Madasamy et al., "Hybrid multicarrier random space vector PWM for the mitigation of acoustic noise," *Electronics*, vol. 10, no. 12, pp. 1483–1483, Jun. 2021.

[14] P. Zhang, S. Wang, and Y. Li, "Performance and analysis of N-state random pulse position SVPWM with constant sampling frequency," *IEEE Trans. Power Electron.*, vol. 37, no. 11, pp. 13606–13625, Nov. 2022.

[15] A. Peyghambari, A. Dastfan, and A. Ahmadyfard, "Selective voltage noise cancellation in three-phase inverter using random SVPWM," *IEEE Trans. Power Electron.*, vol. 31, no. 6, pp. 4604–4610, Jun. 2016.

[16] F. Bu, T. Pu, W. Huang, and L. Zhu, "Performance and evaluation of five-phase dual random SVPWM strategy with optimized probability density function," *IEEE Trans. Ind. Electron.*, vol. 66, no. 5, pp. 3323–3332, May 2019.

[17] Z. Quan and Y. W. Li, "Impact of PWM schemes on the common-mode voltage of interleaved three-phase two-level voltage source converters," *IEEE Trans. Ind. Electron.*, vol. 66, no. 2, pp. 852–864, Feb. 2019.

[18] J. Biswas, M. D. Nair, V. Gopinath, and M. Barai, "An optimized hybrid SVPWM strategy based on multiple division of active vector time (MDAVT)," *IEEE Trans. Power Electron.*, vol. 32, no. 6, pp. 4607–4618, Jun. 2017.
[19] Y. Huang, Y. Xu, W. Zhang, and J. Zou, "Modified single-edge SVPWM technique to reduce the switching losses and increase PWM harmonics frequency for three-phase VSIs," *IEEE Trans. Power Electron.*, vol. 35, no. 10, pp. 10643–10653, Oct. 2020.
[20] Y. Huang, Y. Xu, Y. Li, G. Yang, and J. Zou, "PWM frequency voltage noise cancelation in three-phase VSI using the novel SVPWM strategy," *IEEE Trans. Power Electron.*, vol. 33, no. 10, pp. 8596–8606, Oct. 2018.
[21] X. Han, D. Jiang, T. Zou, R. Qu, and K. Yang, "Two-segment three phase PMSM drive with carrier phase-shift PWM for torque ripple and vibration reduction," *IEEE Trans. Power Electron.*, vol. 34, no. 1, pp. 588–599, Jan. 2019.
[22] M. Su, J. Lin, Y. Sun, and S. Xie, "A new modulation strategy to reduce common-mode current of indirect matrix converter," *IEEE Trans. Ind. Electron.*, vol. 66, no. 9, pp. 7447–7452, Sep. 2019.
[23] B. Wang and E. Sherif, "Spectral analysis of matrix converters based on 3-D Fourier integral," *IEEE Trans. Power Electron.*, vol. 28, no. 1, pp. 19–25, Jan. 2013.
[24] T. Shi, L. Wu, Y. Yan, and C. Xia, "Harmonic spectrum of output voltage for space vector-modulated matrix converter based on triple Fourier series," *IEEE Trans. Power Electron.*, vol. 33, no. 12, pp. 10646–10653, Dec. 2018.
[25] W. Liang, J. Wang, P. C.-K. Luk, W. Fang, and W. Fei, "Analytical modeling of current harmonic components in pmsm drive with voltage-source inverter by SVPWM technique," *IEEE Trans. Energy Convers.*, vol. 29, no. 3, pp. 673–680, Sep. 2014.
[26] D. Xu, M. Yang, Y. Chen, J. Long, and D. Xu, "EMI-regulated SiC-based motor drives with Markov chain pseudo-random frequency space vector pulse width modulation strategy," *IEEE Trans. Energy Convers.*, vol. 37, no. 4, pp. 2348–2358, Dec. 2022.

Yang Yang was born in Shaanxi, China, in 1997. He received the B.S. and M.S. degrees in 2019 and 2022, respectively, from the Xi'an University of Technology, Xi'an, China, where he is currently working toward the Ph.D. degree with the School of Electrical Engineering, all in electrical engineering.

His current research interests include power electronics and ac motor drive control.

Weizhang Song was born in Henan, China, in 1980. He received the B.S. and M.S. degrees in information and control engineering and the Ph.D. degree in electrical engineering from the Xi'an University of Technology, Xi'an, China, in 2004, 2007, and 2010, respectively.

He was with the Department of Electrical Engineering, Xi'an University of Technology, in 2011, where he was a Professor in 2019. From 2014 to 2015, he was a Research Fellow with the Power Electronics, Machines, and Control Group, University of Nottingham, Nottingham, U.K. He is currently the Deputy Dean with the School of Electrical Engineering, Xi'an University of Technology. He has authored and coauthored more than 80 refereed journal and international conference papers. His current research interests include power electronics, ac motor, and its high performance control.

Yang Ge received the Ph.D. degree in electrical engineering from Xi'an Jiaotong University, Xi'an, China, in 2021.

He is currently with Xi'an University of Technology, Xi'an, China. His research interest includes the high-performance control of electric machines.

Patrick Wheeler (Fellow, IEEE) received the B.Eng. (hons.) degree in electrical engineering and the Ph.D. degree in matrix converters from the University of Bristol, Bristol, U.K., in 1994 and 1990, respectively.

In 1993, he was with the University of Nottingham and was a Research Assistant with the Department of Electrical and Electronic Engineering. In 1996, he was a Lecturer with the Power Electronics, Machines, and Control Group, University of Nottingham, U.K. Since January 2008, he has been a Full Professor with the Power Electronics, Machines, and Control Group. He is currently the Director for Global Engagement with the Faculty of Engineering and the Head with the Power Electronics, Machines, and Control Research Group. He was the Head with the Department of Electrical and Electronic Engineering, University of Nottingham, from 2015 to 2018. He has authored and coauthored more than 850 academic publications in leading international conferences and journals.

He is a member of the IEEE Power Electronics Society (IEEE PELS) AdCom and is currently IEEE PELS Vice-President for Technical Operations.